Biochemistry

 Volume 41, Number 2 January 15, 2002

Articles

Chromophore Distortions in the Bacteriorhodopsin Photocycle: Evolution of the H−C14−C15−H Dihedral Angle Measured by Solid-State NMR†

Jonathan C. Lansing,‡ Morten Hohwy,‡,§ Christopher P. Jaroniec,‡ A. F. L. Creemers,|| Johan Lugtenburg,|| Judith Herzfeld,⊥ and Robert G. Griffin*,‡

Department of Chemistry and Center for Magnetic Resonance, Francis Bitter Magnet Laboratory, Massachusetts Institute of Technology, Cambridge, Massachusetts 02139-4307, Leiden Institute of Chemistry, Universiteit Leiden, 2300 RA, Leiden, The Netherlands, and Department of Chemistry and Keck Institute for Cellular Visualization, Brandeis University, Waltham, Massachusetts 02454-9110

Received July 23, 2001; Revised Manuscript Received November 13, 2001

ABSTRACT: In recent years, structural information about bacteriorhodopsin has grown substantially with the publication of several crystal structures. However, precise measurements of the chromophore conformation in the various photocycle states are still lacking. This information is critical because twists about the chromophore backbone chain can influence the Schiff base nitrogen position, orientation, and proton affinity. Here, we focus on the C14−C15 bond, using solid-state nuclear magnetic resonance spectroscopy to measure the H−C14−C15−H dihedral angle. In the resting state (bR_{568}), we obtain an angle of 164 ± 4°, indicating a 16° distortion from a planar all-*trans* chromophore. The dihedral angle is found to decrease to 147 ± 10° in the early M intermediate (M_o) and to 150 ± 4° in the late M intermediate (M_n). These results demonstrate changes in the chromophore conformation undetected by recent X-ray diffraction studies.

Bacteriorhodopsin (bR),[1] the sole protein component of purple membrane, utilizes light energy to create a proton gradient across the cell membrane of *H. salinarum*. Absorption of a photon by the protonated retinylidene chromophore (Figure 1) initiates a cycle in which the Schiff base (SB) releases a proton to Asp85 on the extracellular side of the protein. Subsequently, reprotonation of the SB occurs from the cytoplasmic side by donation of a proton from Asp96. Vectorial proton transport thus depends on a switch in connectivity of the SB nitrogen during the time that it is deprotonated.

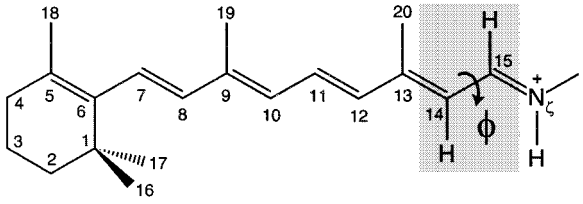

FIGURE 1: Structure of the all-*trans*, 15-anti retinylidene chromophore in light-adapted bacteriorhodopsin. The gray box frames the specifically ^{13}C-labeled H−C14−C15−H moiety.

† This research was supported by NIH Grants GM-36810, GM-23289, and RR-00995. C.P.J. acknowledges the support of a predoctoral fellowship from the National Science Foundation. M.H. is a Human Frontier Science Program postdoctoral fellow.

* To whom correspondence should be addressed. E-mail: rgg@mit.edu, Telephone: 617-253-5597, Fax: 617-253-5405.

‡ Massachusetts Institute of Technology.

§ Present address: Laboratory for Physical Chemistry, ETH-Honggerberg, CH-8093 Zurich, Switzerland.

|| Universiteit Leiden.

⊥ Brandeis University.

10.1021/bi011529r CCC: $22.00
Published on Web 12/15/2001

Discussions of the required change in SB connectivity have emphasized the distinction between a chromophore-based switch and a protein-based switch. In the former, a conformational change in the chromophore moves the SB relative to functional groups in the protein (*1*). In the latter, a protein conformational change rearranges critical functional groups around the SB (*2*). It is important to note that, despite photon-induced isomerization of the chromophore from all-*trans* to 13-*cis* at the start of the photocycle, the SB remains connected to the extracellular side of the protein until the SB becomes deprotonated. This suggests (*3, 4*) that during the first half of the photocycle the protonated SB is restrained by electrostatic interactions in the active site and that the connectivity to the extracellular side of the protein is sustained at the expense of distortions of the chromophore. Such distortions are plausible given the energy that the photon deposits in the chromophore. In fact, FTIR (*5*) and CD (*6, 7*) measurements indicate a nonplanar chromophore already in the resting state. However, intense hydrogen-out-of-plane bending modes indicate an increasing amount of retinal distortion during the first half of the photocycle particularly in the vicinity of C15 (*5, 8*−*11*). These optical results have been largely qualitative and have not been confirmed by X-ray diffraction structures (*12*−*19*), which typically model a planar chromophore structure. (While some small variation of the chromophore from perfect planarity exists in several X-ray structures, comparison of the numerous bR_{568} structures indicates that the dihedral angle of any particular bond is distributed almost uniformly about 180°.)

Early discussions of chromophore twist focused on the single bond closest to the SB. Theoretical calculations suggested that a *cis* C14−C15 bond might be responsible for maintaining the connection of the SB with the extracellular side of the protein during the first half of the photocycle (*1*). However, resonance Raman results did not support the presence of a fully *cis* C14−C15 conformation (*20, 21*). Meanwhile, other spectroscopic results have suggested that double bonds near the SB might be more important. In particular, the intensity of the C15−H out-of-plane wag was taken as a possible indication of twist around the C═N bond (*22*). More recently, NMR results have suggested that one or more double bonds near the SB are strained in the early photocycle and relax while the SB is deprotonated (*23, 24*). The latter timing is consistent with a role in switching the connectivity of the SB (*3, 4*).

Solid-state NMR methods permit quantitative measurements of specific dihedral angles through the correlation of anisotropic interactions. Dipolar couplings are particularly convenient for determining local geometry, as dipolar tensors are oriented along internuclear axes. Correlation of a pair of dipolar interactions yields spectra that depend not only on the size but also on the relative orientation of the couplings, thereby providing a measure of the dihedral angle defined by the interacting nuclei. Methods have been proposed for dihedral angle determination via dipole−dipole correlation in NCCN (*25, 26*), HCCH (*27*), HNCH (*28*), and HNNH (*29*) moieties. This approach provides local structural constraints in biological macromolecules with a precision far surpassing X-ray diffraction methods. Dipole−dipole correlations have been utilized for dihedral angle determination in carbohydrates (*30*), peptides (*25, 26, 29, 31, 32*), and proteins (*33*−*35*).

Application of this approach to the bonds near the SB in bR can provide a detailed assessment of the role of chromophore twist in the connectivity of the ion pump. Here, we focus on the controversial C14−C15 bond, measuring the HCCH dihedral angle in the resting chromophore (where the SB is protonated), in the early M photocycle intermediate (where the SB has just lost its proton), and in the late M photocycle intermediate (where the SB is on the verge of regaining a proton). In the resting state (bR_{568}), we find a somewhat distorted chromophore with a dihedral angle of $|\phi| = 164 \pm 4°$. The distortion increases to $|\phi| = 147 \pm 10°$ in the early M state (M_o) and is essentially the same at $|\phi| = 150 \pm 4°$ in the late M state (M_n).

EXPERIMENTAL PROCEDURES

Preparation of Diammonium [2,2′-$^{13}C_2$]Fumarate. Disodium [2,2′-$^{13}C_2$]fumarate (Isotec, Miamisburg, OH) was dissolved in water and reacted with an excess of hydrochloric acid. The resulting [2,2′-$^{13}C_2$]fumaric acid precipitate was rinsed with ice-cold water to remove the sodium chloride. An excess of ammonium hydroxide was added to the fumaric acid to yield diammonium [2,2′-$^{13}C_2$]fumarate.

bR Sample Preparation. PM fragments were isolated from *H. salinarum* according to the conventional procedure (*36*). Synthesis of doubly ^{13}C-labeled retinal, enriched to 99%, was performed according to procedures described elsewhere (*37*). Incorporation of the [14,15-$^{13}C_2$]retinal was accomplished by bleaching the sample in 0.5 M hydroxylamine and subsequent regeneration of the apoprotein with the labeled retinal as previously described (*38*). Regenerated PM fragments (40 mg) were washed several times in 0.3 M guanidine buffer at pH 10.0. Centrifugation of the suspension at a maximum of 43262*g* for 60 min produced a pellet that was packed into a transparent 5 mm quartz rotor.

Accumulation of bR_{568}. PM samples were light-adapted by illumination in situ for 1−2 h with the full visible spectrum of a 1000 W xenon lamp at 0 °C.

Accumulation of M_o. A sample in the bR_{568} state was cooled to −60 °C and illuminated in situ for 1−2 h with long-wavelength light from a Xenon lamp using a 550 nm cutoff filter.

Accumulation of M_n. A sample in the bR_{568} state was cooled to −20 °C and illuminated in situ with $\lambda > 550$ nm light from a Xenon lamp for 1−2 h.

Solid-State NMR Spectroscopy. Dihedral angles were measured using the HCCH pulse sequence depicted in Figure 2. Following ramped ^{1}H−^{13}C cross-polarization (*39*), the 90° pulse creates longitudinal magnetization. Low-power CW decoupling allows undesired transverse magnetization to dephase during the subsequent rotor period (z-filter). Application of the CMR7 sequence (*40*) generates ^{13}C−^{13}C DQ

[1] Abbreviations: bR, bacteriorhodopsin; NMR, nuclear magnetic resonance; FTIR, Fourier transform infrared; rf, radio frequency; CD, circular dichroism; MCD, magnetic circular dichroism; ORD, optical rotation dispersion; PM, purple membrane; CP, cross-polarization; CW, continuous wave; TPPM, two-pulse phase modulation; DQ, double quantum; SB, Schiff base; bR_{568}, sole component of light-adapted bR and the photon receptor for the proton-motive photocycle; M_o and M_n, photocycle intermediates with a deprotonated Schiff base, the latter a thermal relaxation product of the former; χ^2_ν, reduced chi-square.

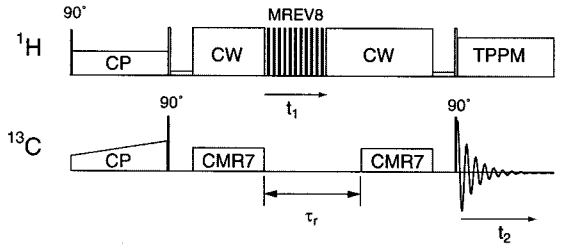

FIGURE 2: Pulse sequence for the HCCH dihedral angle experiment.

coherence between labeled ^{13}C14 and ^{13}C15. The DQ coherence evolves for a total of one rotor period, τ_r, which ensures no net evolution under the anisotropic part of the chemical shift. Centering the carrier between the coupled ^{13}C frequencies results in zero isotropic chemical shift evolution of the DQ coherence. This rotor period is divided into two periods of variable length. During the initial t_1 period, the semi-windowless MREV-8 sequence (*41*, *42*) removes ^{1}H−^{1}H interactions, while retaining scaled ^{1}H−^{13}C heteronuclear couplings. CW decoupling is applied for the remainder of the rotor cycle, which prevents evolution under the ^{1}H−^{13}C couplings. The value of t_1 is incremented from 0 to τ_r in integral steps of the MREV-8 sequence cycle time, for a total of 9 steps. Phase cycling of the CMR7 reconversion step (*43*) selects only magnetization passing through a DQ state and removes all signals from the natural-abundance ^{13}C background. Following an additional z-filter period, a 90° pulse prepares transverse magnetization detectable during t_2.

All experiments were performed using a custom-built spectrometer operating at a ^{1}H frequency of 317.274 MHz. The custom-built triple resonance probe was equipped with a 5 mm Chemagnetics (Fort Collins, CO) spinning module, and sample rotation rates were regulated at 5315 ± 2 Hz. Protein sample temperatures were maintained at −90 °C during all NMR experiments to ensure the stability of the prepared protein states. Proton fields were 100 kHz for TPPM decoupling (*44*), 50 kHz during CP, and 127.6 kHz at all other times. DQ excitation and reconversion using CMR7 were accomplished using ^{13}C fields of 37.2 kHz for 752.64 μs in each step. The CP contact time was 2 ms, and recycle delays of 2 s were utilized. Each t_1 point is the average of 19 000−29 000 transients.

Data Processing. Spectral intensities of the C14 and C15 peaks were extracted from Fourier-transformed experimental data by fitting isotropic lines to pure Gaussian peak shapes. The rotational sideband intensities were within the noise for all but the first and last t_1 points and therefore neglected to avoid fitting random noise. For a given 2D experiment, peak positions and line widths were constrained to a constant value; only peak heights were varied as a function of t_1. Error in the individual intensities was determined to the 90% confidence limit using an F test to determine when the χ^2_ν value for a given fit was significantly larger than the χ^2_ν of the best fit (*45*).

Simulations. Modulation of the sum intensity of the ^{13}C14 and ^{13}C15 signals as a function of t_1 due to the heteronuclear dipolar evolution was simulated using the analytical expression (*27*) which relies on a first-order average Hamiltonian description of the ^{13}C−^{13}C recoupling sequence and the evolution of the spin system in the dipolar dephasing period:

$$a(t_1) = \langle \sin^2[\omega_{DQ}\tau_{DQ}] \prod_\lambda \cos \Psi_\lambda(t_1) \rangle \qquad (1)$$

Here the angle brackets denote signal averaging over all possible molecular orientations, the sine term accounts for the anisotropic DQ excitation, and the cosine terms describe the heteronuclear dipolar dephasing during t_1. The DQ excitation time is denoted τ_{DQ}, and ω_{DQ} is the orientation-dependent scaled ^{13}C−^{13}C dipolar coupling. For a particular time-dependent dipolar coupling λ, the accumulated phase $\Psi_\lambda(t_1)$ is

$$\Psi_\lambda(t_1) = \int_0^{t_1} \kappa\omega_\lambda(t)\, dt \qquad (2)$$

where κ is the scaling factor of the MREV-8 sequence. Expressions for the instantaneous dipolar coupling ω_λ, which depends on the inverse cube of the C−H internuclear distance and the orientation of the coupling in the magnetic field, have been described in detail elsewhere (*27*, *28*). The relative orientation (to be interpreted in terms of dihedral and bond angles) is encoded in the product of cosines, producing distinctive patterns in the indirect dimension. Isotropic chemical shift evolution of the DQ coherence is neglected in this treatment as the sum chemical shift vanishes when the carrier is centered between the recoupled peaks. Anisotropic chemical shift terms do not enter eq 1 as a consequence of the choice of one rotor period, τ_r, for the constant time evolution period.

Four ^{1}H−^{13}C dipolar interactions (the interactions between the labeled ^{13}C nuclei and the two protons bound to them) were modeled in the simulations. Relaxation in the indirect dimension due to insufficient decoupling of ^{1}H−^{1}H interactions was modeled as monoexponential decay. This simple model of relaxation, as well as the first-order approximation represented by eq 1, was justified (vide infra) by comparison to full numerical simulations employing the parameters relevant to our particular experimental setup. Powder averaging was performed using 20 equally distributed γ angles and 256 pairs of α and β crystallite angles generated by the REPULSION method (*46*). Increasing the number of crystallites beyond this point did not change the result significantly. The assumption of 115° bond angles in the simulations was based upon the X-ray crystal structure of *all-trans*-retinal (*47*). Retinal C15−H and C14−H bond lengths were assumed to correspond to standard C−H bond lengths. Accordingly, the scaled ^{13}C−^{1}H dipolar couplings were set to the value of 12.3 kHz measured for the C_α−H bonds of [2-^{13}C,^{15}N]leucine in a DIPSHIFT experiment (*48*). These geometric assumptions were determined to be reasonable by additional simulations (vide infra).

Error Analysis. The influence of long-term variations in the experiments from sources such as temperature fluctuations and amplifier instability was minimized by collecting data in an interleaved fashion, with 256 transients recorded per t_1 point in each pass through the entire indirect dimension. The best fit to model conformations was determined by minimizing χ^2_ν, with the weighting of each point determined by the error in fitting of the spectral peaks. Confidence limits for the dihedral angles were determined using an F test at the 90% confidence level, where the normalization of the

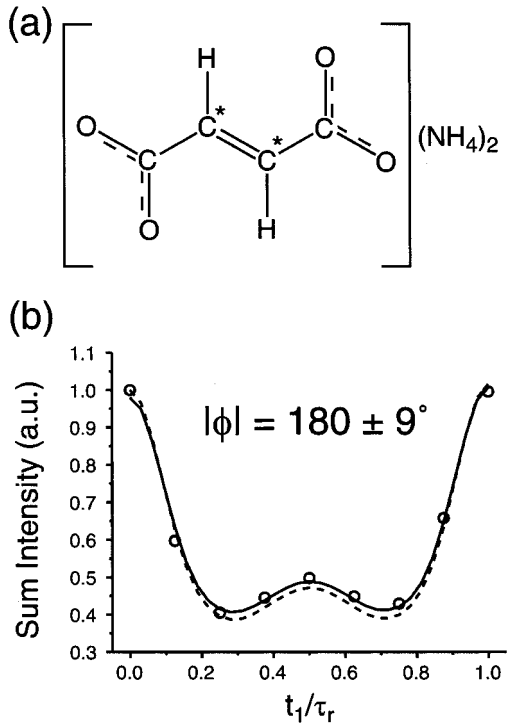

FIGURE 3: (a) Structure of diammonium fumarate. The asterisks denote the ^{13}C-labeled 2 and 2′ positions. (b) Modulation of the double-quantum-filtered intensity upon varying the fraction of the rotor period with dipolar evolution. The solid line denotes the best fit at $\phi = 180°$, and the dashed line represents the 90% confidence limit. The experimental data were collected under the same conditions listed under Experimental Procedures for bR, except that the sample temperature was maintained at 20 °C.

initial point, the relaxation rate, and the dihedral angle were the only free parameters.

RESULTS

Proper performance of the HCCH dihedral angle measurement was verified using diammonium [2,2′-$^{13}C_2$]fumarate (Figure 3a). The best fit to the experimental data at $\phi = 180°$ (Figure 3b) agrees perfectly with the X-ray crystal structure (*49*) and previous NMR results (*27*). Digitization of the dipolar evolution dimension into 9 points at $\nu_r = 5315$ Hz results in an uncertainty of ±9° with only a minimal amount of experimental noise. The angular uncertainty in this measurement of the conformation of diammonium fumarate is limited principally by the small variation between dephasing curves for conformations within a few degrees of *trans*. Simulations indicate that the optimal angular resolution occurs for $|\phi|$ in the range from 175 to 140°, with substantially worse resolution for conformations with $|\phi| < 140°$.

Comparison of the CP and double-quantum-filtered spectra of [14,15-$^{13}C_2$]retinal bR (Figure 4) illustrates the high efficiency (~50%) of the double-quantum excitation. High-quality proton decoupling is critical for the proper performance of the DQ mixing sequence. Maintenance of a 3-fold or greater mismatch between the ^1H and ^{13}C fields is advisable for optimum DQ efficiency (*50, 51*). Insufficient proton decoupling during the recoupling sequence not only reduces the available signal, but also leads to selection of only those crystallite orientations that correspond to weak

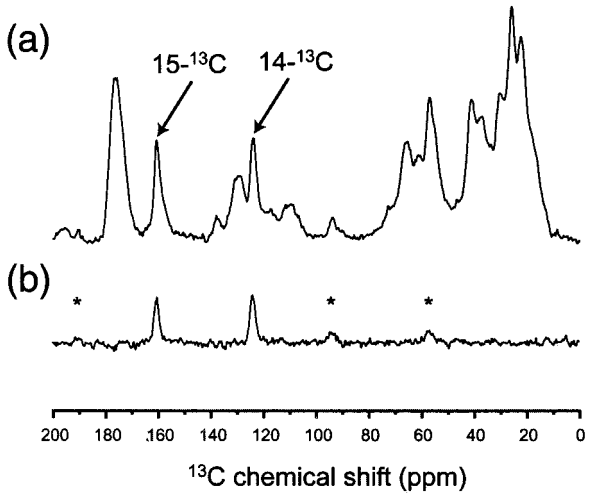

FIGURE 4: (a) Cross-polarization and (b) double-quantum-filtered spectra of [14,15-$^{13}C_2$]retinylidene bR. Natural-abundance ^{13}C signals vanish in (b) due to the DQ filtration. Asterisks identify rotational sidebands of the labeled peaks.

Table 1: Measured Values of the H−C14−C15−H Dihedral Angle of Bacteriorhodopsin in Various States

state	$\|\phi\|$
bR_{568}	164 ± 4°
M_o	147 ± 10°
M_n	150 ± 4°

$^{13}C-^1H$ couplings, and the accuracy of the expression for the excitation profile (eq 1) may be strongly compromised. The respectable DQ efficiency in bR, compared to a theoretical maximum of 73%, justifies the usage of the analytical expression for the excitation profile of the $^{13}C-^{13}C$ recoupling sequence.

HCCH magnetization trajectories for the bR_{568}, M_o and M_n states are presented in Figure 5 with the best-fitting simulations. The values of $|\phi|$ for each state are presented with confidence limits in Table 1. In all cases, signal loss during the $^{13}C-^1H$ dephasing period is very modest (78−96% of the intensity remaining in the last t_1 points), indicating the high quality of the homonuclear decoupling during the MREV-8 sequence.

The dashed line in Figure 5a represents the simulation for $\phi = 180°$. The large deviation from the experimental data demonstrates that the chromophore conformation cannot be mistaken for planar. The deviation from planarity increases for the two M states. Asymmetry in the magnetization trajectory measured for the M_o state (most notable in the 6th time point) appears to be due to random noise and is responsible for the increased uncertainty in the M_o conformation. However, it is clear that the bR_{568} conformation is distinctly different from the deprotonated M states and that none of these states possesses a planar configuration of the C14−C15 bond.

Fitting the experimental data required several assumptions about the bond angles, bond lengths, and relaxation rates. The validity of these assumptions was verified through additional simulations, and no significant errors were associated with these parameters.

The influence of H−C−C bond angles upon the HCCH magnetization trajectory was found to be small when the dihedral angle was in the range of 120−180°. Variation of

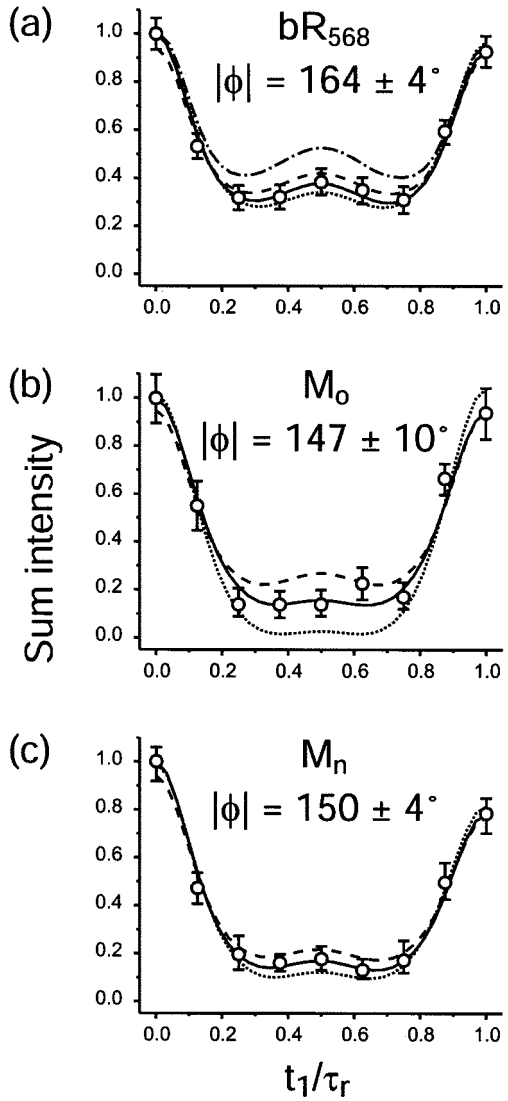

FIGURE 5: Dephasing curves for the HCCH dihedral angle measurement of (a) bR_{568}, (b) M_o, and (c) M_n forms of [14,15-$^{13}C_2$]retinylidene bR. Error bars indicate the 90% confidence limits for the data points. Solid lines represent the best fit to each data set. Dashed and dotted lines denote the upper and lower confidence limits for each state, respectively. A simulation (dash−dot) for $\phi = 180°$ is presented in (a).

the bond angles by 2° altered the best-fitting dihedral angle by less than 2°. In the *trans* conformation, the dipolar couplings remain collinear no matter how much symmetric variation is applied to the H−C−C bond angles. For dihedral angles close to the *cis* conformation, 2° variations in the bond angle had more significant effects (ca. 6−8° deviations) on the dihedral angle fitting routine.

The length of the C14−C15 bond influences the $^{13}C-^{13}C$ coupling utilized in the CMR7 mixing steps and the weaker two-bond $^{13}C-^{1}H$ couplings. Simulations of the measurements on all three states were performed using a bond length of 1.46 Å derived from the crystal structure of retinal (*47*) and in close agreement with the QM/MM structure calculation of bR_{568} (*52*). Ab initio calculations suggest bond length changes upon bond rotation or SB deprotonation are small (*53*). Simulations of the dephasing trajectory in t_1 indicate that these experiments have only a weak dependence upon the magnitude and orientation of the two-bond $^{13}C-^{1}H$ couplings. Likewise, the anisotropy of the CMR7 mixing sequence is only modestly perturbed by small changes in the $^{13}C-^{13}C$ coupling magnitude. Even assuming the C14−C15 bond length changed by as much as 0.1 Å, this perturbation would alter the measured dihedral angle by less than 1°, an effect much smaller than the influence of random noise.

The effect of varying the $^{13}C-^{1}H$ coupling magnitudes, equivalent to changing the bond lengths, was also investigated. The HCCH experiment was found to be relatively insensitive to the size of the dipolar interactions, as long as the two strong interactions are of approximately equal size. Variations of up to 10% in the coupling magnitude (equivalent to a 3% variation of the bond length) did not alter the best-fitting dihedral angle, but the error limits broadened as the coupling strength was purposely misset. The shape of the dephasing trajectory in the near-*trans* limit is principally determined by the dihedral angle and is much less dependent on the magnitude of the couplings. When the scaled dipolar coupling was allowed to vary freely in the fitting routines, the optimal fits indicated a scaled coupling equal to that measured in [2-^{13}C,^{15}N]leucine, validating the assumptions made in the initial simulations. The insensitivity of the HCCH dihedral angle measurement to the scaled coupling magnitudes was previously demonstrated in fitting carbohydrate dipolar correlation data without independent measurement of scaling factor κ (*30*).

The relaxation model used in simulating the experimental data assumes that the relaxation rates of pure ^{13}C transverse spin state and the product states involving ^{1}H states during t_1 are equivalent. While this assumption is not generally valid, the monoexponential decay fits well for times that are small compared to the time scale of the relaxation ($t \ll T_2$). Test calculations demonstrated that full spin simulations of the experiment including differential relaxation gave essentially the same results as the analytical expression in eq 1, with no significant improvement in the fit quality to justify the use of the additional fit parameter. However, the monoexponential model is not expected to be valid when the magnetization trajectory is monitored for longer times (*54*) or when the relaxation rate is not small compared to the sample rotation rate.

Only four heteronuclear couplings were considered in the simulations, corresponding to all possible $^{1}H-^{13}C$ couplings in the four-spin system consisting of the labeled ^{13}C nuclei and their directly bonded protons. For a deprotonated chromophore, this model accurately represents all the significant heteronuclear couplings to the $^{13}C14-^{13}C15$ spin pair. While protons of the C20 methyl group, amino acid side chains, and presumably water are also present, these couplings will be significantly smaller than the one- and two-bond couplings, and will not evolve significantly over the course of a rotor period. As a result, these long-range couplings have little effect on the magnetization trajectory.

A protonated chromophore has an additional two-bond $^{1}H_N-^{13}C15$ coupling, of comparable magnitude to the two-bond $^{1}H14-^{13}C15$ and $^{1}H15-^{13}C14$ couplings. The precise orientation of this dipolar interaction is not known, as it has been suggested that the dihedral angle about the N═C15 bond is distorted from 180° (*52*, *55*). However, assuming typical bond lengths, bond angles, and an H−N−C15−H dihedral angle close to 180° restricts the possible orientations

of this coupling to a small region. To assess the importance of this third two-bond coupling, a series of simulations were performed for five-spin systems of geometries corresponding to a protonated [14,15-$^{13}C_2$] chromophore over the full range of C14−C15 dihedral angles and several possible $^1H_N-^{13}C15$ dipole orientations. The magnetization trajectory was only slightly distorted by the $^1H_N-^{13}C15$ coupling with respect to the four-spin simulations. The trajectories were insensitive to the exact $^1H_N-^{13}C15$ dipole orientation. The dihedral angle could be faithfully extracted from the five-spin magnetization trajectories using the simple four-spin model except at geometries extremely close to the ideal *cis* or *trans* conformation. For $|\phi| > 175°$, the four-spin model underestimates the dihedral angle by 2−3°. A 1° underestimation of $|\phi|$ occurred for dihedral angles between 175° and 165°. For $|\phi|$ between 165° and 35°, the four-spin model faithfully reproduces the correct dihedral angle. The overestimation of the dihedral angle gradually increases as one approaches the *cis* conformation, with a maximum error of 9° at $\phi = 0°$. Therefore, neglect of the $^1H_N-^{13}C15$ dipole coupling is justified over the range of geometries expected for the C14−C15 bond of the chromophore.

We find that the HCCH dipolar correlation experiment is superbly suited for dihedral angle measurements in the near-*trans* regime. Of all the structural parameters, the HCCH signal dephasing depends on the dihedral angle most strongly. Bond length variations (as reflected in the dipolar coupling magnitudes), symmetric bond angle changes, and long-range $^1H-^{13}C$ couplings are found to have less influence on the dihedral angle measurement than experimental noise.

DISCUSSION

The simulated fits of the bR_{568} results (Figure 5a) indicate a dihedral angle of 164 ± 4°. This represents a significant deviation from the ideal planar conformation of free *all-trans*-retinal. Thus, even the relaxed ground-state structure incorporates a distorted chromophore. This result confirms the analysis of FTIR (*5*), CD (*6*, *7*), MCD (*6*), and ORD (*56*) experiments. The optical studies specifically indicated nonplanarity in the region of the C14−C15 bond of bR_{568}. A distortion of the C14−C15 bond also explains why the strongest hydrogen-out-of-plane bending mode in the bR_{568} chromophore is at C14 in resonance Raman measurements (*20*). The distortion of the C14−C15 bond suggests that the bR_{568} chromophore is "spring-loaded" in preparation for the initial photon-driven isomerization event, although the functional role of this tension is unclear.

Deprotonation of the chromophore strengthens bond order alternation along the polyene chain, thereby decreasing the barrier to rotation about the C14−C15 bond. As shown in Figure 5b, we find that the C14−C15 bond becomes more distorted by the M_o state, with a dihedral angle of ±147°. The asymmetry in the M_o data appears to be due to random noise and leads to the increased uncertainty in the ϕ value. Despite changes in the $^{13}C14$ and SB ^{15}N chemical shifts (*38*), no significant change in the H−C14−C15−H dihedral angle occurs in the $M_o \rightarrow M_n$ transition.

A variety of pulse sequences have been developed to measure torsion angles by correlating a pair of proton heteronuclear dipolar couplings (*27*, *28*) or by correlating a proton heteronuclear dipolar coupling with a chemical shift tensor (*57*, *58*). The direct result of these techniques is the determination of an H−X−Y−H or H−X−Y−Z dihedral angle (X, Y, Z ∈ {C, N}). Typically, the results for the light atom positions are related to a torsion angle, such as the peptide backbone ϕ and ψ angles, defined by the positions of the heavy atom substituents. This relation requires assumptions about the relative orientations of the protons and heavy atom substituents. For peptide backbone conformations, in particular, it is generally assumed that amide groups are perfectly planar and that C_α and side chain carbons are perfectly tetrahedrally coordinated. However, this is not in complete agreement with experimental determinations. For example, neutron diffraction structures of glycylglycine (*59*−*62*) indicate an amide hydrogen position that is 3−8° out of the peptide plane. The geometry at C_α positions is also distorted from tetrahedral in neutron diffraction structures of glycylglycine (*59*−*62*) and various amino acids (*63*−*69*). These data suggest that the translation of proton-dependent dihedral angles into heavy atom dihedral angles can add an additional uncertainty of 5−8° for each proton used.

Along the polyene chain of retinal, the expectation for distortions of the proton positions is lower. Unlike the sp^3 carbons of peptide side chains, the protonated retinal SB forms a conjugated π system that places restraints upon the proton orientations. X-ray diffraction structures (*12*, *13*, *16*) and calculated structures from molecular dynamics (*55*) and hybrid quantum mechanics/molecular mechanics calculations (*52*) of bR_{568} do not indicate packing about the C14−C15 bond that would sterically induce a distortion of the proton positions. Thus, it seems likely that the determination of $|\phi| = 164°$ in bR_{568} indicates a rotation of the C14−C15 bond that partially disrupts the conjugation of the π system.

However, recent hybrid quantum mechanical/molecular mechanical calculations for bR_{568} (*52*) suggest an alternative interpretation of our results. These calculations predict an H−C14−C15−H dihedral angle of 165°, in excellent agreement with our determination, but with a C13−C14−C15−N dihedral angle of 179°. This unusual geometry is part of a twisted region of the chromophore extending from C13 to the SB nitrogen. Both of these interpretations are consistent with the H−C14−C15−H dihedral angle measured in bR_{568}. Experimental measurements of the C13−C14−C15−N dihedral angle are underway and should clarify its relationship to the HCCH dihedral angle.

For the deprotonated M states, the most likely interpretation of the HCCH dihedral angle is a rotation of the C14−C15 bond. Deprotonation of the SB nitrogen neutralizes the positive charge and increases the bond order alternation along the polyene chain. As a result, the barrier to C14−C15 bond rotation should decrease. The magnitude of the deviation of $|\phi|$ from 180° also argues for bond rotation, as rather dramatic deviations from planarity about C14 and C15 would be required to produce a $|\phi|$ value of 150°.

Thus, we find that the chromophore starts the photocycle with a distorted C14−C15 bond, although it remains to be established whether this distortion is limited to the proton positions or a complete twist of the C14−C15 bond. By the time that the SB has deprotonated, the C14−C15 bond has rotated to adopt a conformation 30° away from a planar *trans* conformation.

CONCLUSIONS

The light-adapted chromophore in bR_{568} is distorted about the C14−C15 bond, with an HCCH dihedral angle of ±164°. This result indicates that the protons of the C14−C15 moiety are twisted out of the plane of the chromophore, although the possibility that the heavy atoms of the bR_{568} chromophore remain in-plane cannot be excluded at this point. This strain at the C14−C15 bond suggests that the chromophore is in an activated or preloaded state at the start of the photocycle.

The distortion around the C14−C15 bond is greater in the M intermediates where the HCCH angle is ±150°. This additional distortion may help the SB to remain connected to the extracellular side of the protein during the first half of the photocycle. However, the distortion of the H−C14−C15−H conformation remains constant while the SB is deprotonated. Thus, rotation of the C14−C15 bond does not appear to contribute to the change in connectivity to the cytoplasmic side of the protein that occurs while the SB is deprotonated. This is consistent with evidence that it is distortion around one or more nominal double bonds (e.g., the neighboring C13═C14 and C15═N bonds) that is released while the SB is deprotonated (*3*, *4*, *23*, *24*). Experiments are underway to measure dihedral angles around these bonds with a view to assessing their role in the connectivity switch.

The reported results demonstrate the presence of small-scale changes of the chromophore conformation during the photocycle that have not been detected in X-ray diffraction studies. Thus, in considering the mechanistic implications of X-ray structures, the possibility of undetected changes in local structure should be kept in mind. Although small in scale, these changes may be functionally significant because chromophore twists provide a possible mechanism by which bR can modulate the pK_a of the SB nitrogen and its interaction with proton donor and acceptor groups. Further investigation of the chromophore conformation of photocycle intermediates is warranted to elucidate the proton pumping mechanism of bacteriorhodopsin.

ACKNOWLEDGMENT

We thank Chad M. Rienstra for helpful discussions and S. Hiyashi and I. Ohmine for providing the bR coordinates from their simulations.

REFERENCES

1. Schulten, K., and Tavan, P. (1978) *Nature 272*, 85−86.
2. Fodor, S. P. A., Ames, J. B., Gebhard, R., van den Berg, E. M. M., Stoeckenius, W., Lugtenburg, J., and Mathies, R. A. (1988) *Biochemistry 27*, 7097−7101.
3. Herzfeld, J., and Lansing, J. C. (2001) *Annu. Rev. Biomol. Struct.* (in press).
4. Herzfeld, J., and Tounge, B. A. (2000) *Biochim. Biophys. Acta 1460*, 95−105.
5. Fahmy, K., Siebert, F., Grosjean, M. F., and Tavan, P. (1989) *J. Mol. Struct. 214*, 257−288.
6. El-Sayed, M. A., Lin, C. T., and Mason, W. R. (1989) *Proc. Natl. Acad. Sci. U.S.A. 86*, 5376−5379.
7. Wu, S., and El-Sayed, M. A. (1991) *Biophys. J. 60*, 190−197.
8. Rodig, C., Chizhov, I., Weidlich, O., and Siebert, F. (1999) *Biophys. J. 76*, 2687−2701.
9. Maeda, A., Sasaki, J., Pfefferle, J.-M., Shichida, Y., and Yoshizawa, T. (1991) *Photochem. Photobiol. 54*, 911−921.
10. Doig, S. J., Reid, P. J., and Mathies, R. A. (1991) *J. Phys. Chem. 95*, 6372−6379.
11. Pfefferle, J.-M., Maeda, A., Sasaki, J., and Yoshizawa, T. (1991) *Biochemistry 30*, 6548−6556.
12. Belrhali, H., Nollert, P., Royant, A., Menzel, C., Rosenbusch, J. P., Landau, E. M., and Pebay-Peyroula, E. (1999) *Structure 7*, 909−917.
13. Essen, L.-O., Siegert, R., Lehmann, W. D., and Oesterhelt, D. (1998) *Proc. Natl. Acad. Sci. U.S.A. 95*, 11673−11678.
14. Luecke, H., Richter, H.-T., and Lanyi, J. K. (1998) *Science 280*, 1934−1937.
15. Luecke, H., Schobert, B., Richter, H.-T., Cartailler, J.-P., and Lanyi, J. K. (1999) *Science 286*, 255−260.
16. Luecke, H., Schobert, B., Richter, H.-T., Cartailler, J.-P., and Lanyi, J. K. (1999) *J. Mol. Biol. 291*, 899−911.
17. Edman, K., Nollert, P., Royant, A., Belrhali, H., Pebay-Peyroula, E., Hajdu, J., Neutze, R., and Landau, E. M. (1999) *Nature 401*, 822−826.
18. Sass, H. J., Buldt, G., Gessenich, R., Hehn, D., Neff, D., Schlesinger, R., Berendzen, J., and Ormos, P. (2000) *Nature 406*, 649−653.
19. Royant, A., Edman, K., Ursby, T., Pebay-Peyroula, E., Landau, E. M., and Neutze, R. (2000) *Nature 406*, 645−648.
20. Smith, S. O., Braiman, M. S., Myers, A. B., Pardoen, J. A., Courtin, J. M. L., Winkel, C., Lugtenburg, J., and Mathies, R. A. (1987) *J. Am. Chem. Soc. 109*, 3108−3125.
21. Ames, J. B., Fodor, S. P. A., Gebhard, R., Raap, J., van den Berg, E. M. M., Lugtenburg, J., and Mathies, R. A. (1989) *Biochemistry 28*, 3681−3687.
22. Gat, Y., Grossjean, M., Pinevsky, I., Takei, H., Rothman, Z., Sigrist, H., Lewis, A., and Sheves, M. (1992) *Proc. Natl. Acad. Sci. U.S.A. 89*, 2434−2438.
23. Hatcher, M. E., Hu, J. G., Belenky, M., Verdegem, P., Lugtenburg, J., Griffin, R. G., and Herzfeld, J. (2001) *Biophys. J.* (in press).
24. Hu, J. G., Sun, B. Q., Petkova, A. T., Griffin, R. G., and Herzfeld, J. (1997) *Biochemistry 36*, 9316−9322.
25. Feng, X., Eden, M., Brinkmann, A., Luthman, H., Eriksson, L., Graslund, A., Antzutkin, O. N., and Levitt, M. H. (1997) *J. Am. Chem. Soc. 119*, 12006−12007.
26. Costa, P. R., Gross, J. D., Hong, M., and Griffin, R. G. (1997) *Chem. Phys. Lett. 280*, 95−103.
27. Feng, X., Lee, Y. K., Sandstrom, D., Eden, M., Maisel, H., Sebald, A., and Levitt, M. H. (1996) *Chem. Phys. Lett. 257*, 314−320.
28. Hong, M., Gross, J. D., and Griffin, R. G. (1997) *J. Phys. Chem. B 101*, 5869−5974.
29. Reif, B., Hohwy, M., Jaroniec, C. P., Rienstra, C. M., and Griffin, R. G. (2000) *J. Magn. Reson. 145*, 132−141.
30. Ravindranathan, S., Feng, X., Karlsson, T., Widmalm, G., and Levitt, M. H. (2000) *J. Am. Chem. Soc. 122*, 1102−1115.
31. Nomura, K., Takegoshi, K., Terao, T., Uchida, K., and Kainosho, M. (1999) *J. Am. Chem. Soc. 121*, 4064−4065.
32. Rienstra, C. M., Hohwy, M., Mueller, L. J., Jaroniec, C. P., Reif, B., and Griffin, R. G. (2001) *J. Am. Chem. Soc.* (submitted for publication).
33. Hong, M. (1999) *J. Magn. Reson. 139*, 389−401.
34. Feng, X., Verdegem, P. J. E., Lee, Y. K., Sandstrom, D., Eden, M., Bovee-Geurts, P., de Grip, W. J., Lugtenburg, J., de Groot, H. J. M., and Levitt, M. H. (1997) *J. Am. Chem. Soc. 119*, 6853−6857.
35. Feng, X., Verdegem, P. J. E., Eden, M., Sandstrom, D., Lee, Y. K., Bovee-Geurts, P. H. M., de Grip, W. J., Lugtenburg, J., de Groot, H. J. M., and Levitt, M. H. (2000) *J. Biomol. NMR 16*, 1−8.
36. Oesterhelt, D., and Stoeckenius, W. (1973) *Methods Enzymol. 31*, 667−678.
37. Pardoen, J. A., Winkel, C., Mulder, P. P. J., and Lugtenburg, J. (1984) *Recl. Trav. Chim. Pays-Bas 103*, 135−141.
38. Hu, J. G., Sun, B. Q., Bizounok, M., Hatcher, M. E., Lansing, J. C., Raap, J., Verdegem, P. J. E., Lugtenburg, J., Griffin, R. G., and Herzfeld, J. (1998) *Biochemistry 37*, 8088−8096.
39. Metz, G., Wu, X., and Smith, S. O. (1994) *J. Magn. Reson. A 110*, 219−227.

40. Rienstra, C. M., Hatcher, M. E., Mueller, L. J., Sun, B., Fesik, S. W., and Griffin, R. G. (1998) *J. Am. Chem. Soc. 120*, 10602−10612.
41. Rhim, W.-K., Elleman, D. D., and Vaughan, R. W. (1973) *J. Chem. Phys. 59*, 3740−3749.
42. Mansfield, P. (1971) *J. Phys. C: Solid State Phys. 4*, 1444−1452.
43. Wokaun, A., and Ernst, R. R. (1977) *Chem. Phys. Lett. 52*, 407−412.
44. Bennett, A. E., Rienstra, C. M., Auger, M., Lakshmi, K. V., and Griffin, R. G. (1995) *J. Chem. Phys. 103*, 6951−6958.
45. Bevington, P. R. (1969) *Data Reduction and Error Analysis for the Physical Sciences*, McGraw-Hill, New York.
46. Bak, M., and Nielsen, N. C. (1997) *J. Magn. Reson. 125*, 132−139.
47. Hamanaka, T., Mitsui, T., Ashida, T., and Kakudo, M. (1972) *Acta Crystallogr., Sect. B 28*, 214−222.
48. Munowitz, M., Aue, W. P., and Griffin, R. G. (1982) *J. Chem. Phys. 77*, 1686−1689.
49. Hosomi, H., Ito, Y., and Ohba, S. (1998) *Acta Crystallogr., Sect. C 54*, 142−145.
50. Bennett, A. E., Rienstra, C. M., Griffiths, J. M., Zhen, W., Lansbury, P. T., Jr., and Griffin, R. G. (1998) *J. Chem. Phys. 108*, 9463−9479.
51. Ishii, Y., Ashida, J., and Terao, T. (1995) *Chem. Phys. Lett. 246*, 439−445.
52. Hiyashi, S., and Ohmine, I. (2000) *J. Phys. Chem. B 104*, 10678−10691.
53. Tajkhorshid, E., Paizs, B., and Suhai, S. (1999) *J. Phys. Chem. B 103*, 4518−4527.
54. Hohwy, M., Jaroniec, C. P., Reif, B., Rienstra, C. M., and Griffin, R. G. (2000) *J. Am. Chem. Soc. 122*, 3218−3219.
55. Tajkhorshid, E., Baudry, J., Schulten, K., and Suhai, S. (2000) *Biophys. J. 78*, 683−693.
56. Volkov, V., Svirko, Y. P., Kamalov, V. F., Song, L., and El-Sayed, M. A. (1997) *Biophys. J. 73*, 3164−3170.
57. Hong, M., Gross, J. D., Hu, W., and Griffin, R. G. (1998) *J. Magn. Reson. 135*, 169−177.
58. Ishii, Y., Terao, T., and Kainosho, M. (1996) *Chem. Phys. Lett. 256*, 133−140.
59. Freeman, H. C., Paul, G. L., and Sabine, T. M. (1970) *Acta Crystallogr., Sect. B 26*, 925−932.
60. Koetzle, T. F., Hamilton, W. C., and Parthasarathy, R. (1972) *Acta Crystallogr., Sect. B 28*, 2083−2090.
61. Kvick, A., Al-Karaghouli, A. R., and Koetzle, T. F. (1977) *Acta Crystallogr., Sect. B 33*, 3796−3801.
62. Griffin, J. F., and Coppens, P. (1975) *J. Am. Chem. Soc. 97*, 3496−3505.
63. Al-Karaghouli, A. R., and Koetzle, T. F. (1975) *Acta Crystallogr., Sect. B 31*, 2461−2465.
64. Frey, M. N., Lehmann, M. S., Koetzle, T. F., and Hamilton, W. C. (1973) *Acta Crystallogr., Sect. B 29*, 876−884.
65. Fuess, H., Hohlwein, D., and Mason, S. A. (1977) *Acta Crystallogr., Sect. B 33*, 654−659.
66. Gupta, S. C., Sequeira, A., and Chidambaram, R. (1974) *Acta Crystallogr., Sect. B 30*, 562.
67. Jones, D. D., Bernal, I., Frey, M. N., and Koetzle, T. F. (1974) *Acta Crystallogr., Sect. B 30*, 1220−1227.
68. Lehmann, M. S., Koetzle, T. F., and Hamilton, W. C. (1972) *J. Am. Chem. Soc. 94*, 2657−2660.
69. Lehmann, M. S., Koetzle, T. F., and Hamilton, W. C. (1972) *Int. J. Pept. Protein Res. 4*, 229−239.

BI011529R